

# Ion sensitive field effect transistor modelling for multidomain simulation purposes

Marcin Janicki\*, Marcin Daniel, Michal Szermer, Andrzej Napieralski

*Department of Microelectronics and Computer Science, Technical University of Lodz, Al. Politechniki 11, 93-590 Lodz, Poland*

Received 31 December 2003; received in revised form 24 March 2004; accepted 18 June 2004  
Available online 28 July 2004

## Abstract

The proper design and simulation of modern electronic microsystems oriented towards environment monitoring requires accurate models of various ambient sensors. In particular, this paper presents a comprehensive model of an ion sensitive field effect transistor (ISFET). The model can be employed straightforwardly for simulations at device, circuit or system level.

First, the model was validated with electrical measurements and simulations of real structures performed for different ion concentration and temperature values. Then, the ISFET sensor model was employed for mixed-signal simulations in VHDL-AMS, when the analysis of a microsystem consisting of the ISFET sensor and a sigma–delta analogue-to-digital converter was carried out. Additionally, the presence of other ions than hydrogen in the measured solution was also taken into account in the simulations.

© 2004 Elsevier Ltd. All rights reserved.

*Keywords:* Ion sensitive field effect transistor; Sigma–delta ADC; Multidomain simulations

## 1. Introduction

Modern electronic microsystems often comprise various sensors whose operation principle is based on different physical phenomena not necessarily purely electrical ones. Specialised networks dedicated for continuous monitoring of air, water and soil pollution, which are currently under development in many industrialised countries, might serve as good examples of such microsystems. For the computer aided design of these complex systems, engineers need adequate device models and simulation tools rendering a possible multidomain simulation. This paper illustrates the above problem based on the particular example of an ion sensitive field effect transistor (ISFET), which is commonly employed to measure the concentration of different ions. The proposed ISFET model combines the conventional metal-oxide-semiconductor field effect transistor (MOS-FET) model with a complex electro–chemical gate model. This model, validated with electrical measurements, is implemented then in the newly introduced VHDL-AMS

(Very high speed hardware description language-analogue mixed-signals) standard and simulated together with the sigma–delta analogue-to-digital converter ( $\Sigma$ – $\Delta$  ADC).

The research presented here is a part of a larger international project SEWING-System for European Water monitorING, supported by the 5th Framework Programme of the European Union, aimed at the creation of a water pollution monitoring system. The ISFETs, sensitive to the hydrogen ion concentration, will constitute in this project the common base for all the developed ion concentration sensors. The transistor sensitivity to other ions can be achieved by covering the gate dielectric material with a special ion-selective membrane. Finally, the sensors are to be integrated with a data acquisition unit, which will transmit the pre-processed data to a water quality monitoring station gathering information from all the field posts. There, if necessary, appropriate actions will be undertaken according to sensor indications.

The contents of this paper can be divided in two parts: a theoretical and an experimental one. The first part consists of three sections, which cover briefly the theoretical background concerning the ISFET operation principle and its coupled electro–thermo–chemical model employed by

\* Corresponding author. Tel.: +48-42-6312645; fax: +48-42-6360327.  
E-mail address: janicki@dmc.s.p.lodz.pl (M. Janicki).

the authors in the subsequent simulations. Then, in the experimental part, the results of electrical measurements obtained for two different ISFET device structures are compared with simulations providing the data necessary for model parameter extraction. Finally, the validated device models are used in the multidomain VHDL-AMS simulations of a more complex system.

## 2. Operation principle

Essentially, the ISFET construction is the same as the one of an ordinary MOSFET, except for the fact that the standard metal-polysilicon-dielectric gate is replaced by a more complex structure sensitive to hydrogen ion concentration. Namely, the gate structure, presented in Fig. 1, consists of a reference electrode and a dielectric between which an electrolyte is flowing. The ion concentration in the electrolyte influences the gate potential, which in turn modifies the transistor threshold voltage. In this way, the hydrogen ion concentration exercises an electrostatic control on the drain-source current. The ISFETs are usually operated under the constant drain current mode, which means that the change of the drain current due to the change of the ion concentration in the electrolyte is compensated for by the adjustment of the reference electrode potential (the gate voltage).

Therefore, the ISFET sensitivity is usually expressed as the gate voltage change per a decade of the hydrogen ion concentration pH, i.e. the change of the concentration by 10 times. Note that pH denotes  $-\log[\text{H}^+]$ , e.g. if the value of the pH is equal to 2, the concentration of the hydrogen ions amounts to  $10^{-2}$  mole per litre.

The ISFET sensitivity depends mainly on the choice of the gate dielectric material. The most commonly used materials are silicon and metal oxides or nitrides. Although among these materials especially high sensitivity to the hydrogen ion concentration exhibits the aluminium oxide, because of the technological compatibility reasons, the particular ISFETs investigated in this paper had gates

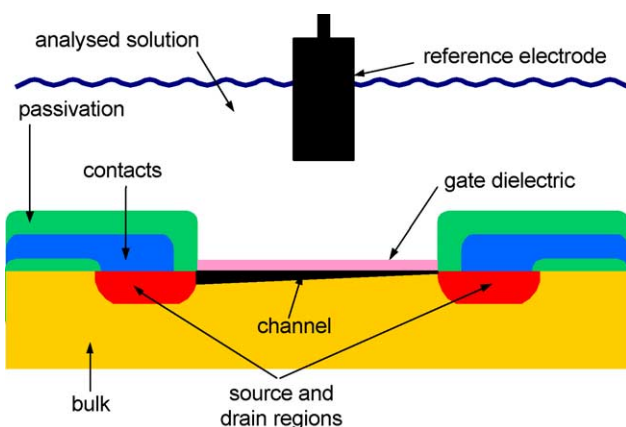


Fig. 1. Cross-section of ISFET structure.

composed of two 50 nm thick layers of silicon nitride and oxide. The theoretical sensitivity of such gates amounts to 59 mV per decade of the hydrogen ion concentration.

When the transistor gate is coated with some ion selective membrane and the so-called PolyHEMA layer stabilising the operation of the sensor, the ISFETs can be used for the selective detection of various species in the surrounding electrolyte, other than the hydrogen ions. Such devices are known as the CHEMically Modified Field Effect Transistors (CHEMFETs).

## 3. Solid–liquid interface model

The theoretical studies of the phenomena occurring at the solid–liquid interface in the ISFET sensors (in the case considered here, it is the interface between the gate dielectric and the electrolyte) had been undertaken by many authors [1–3]. Usually, the ISFET operation is explained by so-called Site-Binding Theory, which relates the interface potential to the concentration of the hydrogen ions in the analysed solution. According to this theory, the ions present in the solution react with positively or negatively charged active sites at the dielectric surface creating hydrogen-active site pairs and consequently changing the total value of the active site charge at the insulator surface. This, in turn, influences the transistor channel current through the variation of the threshold voltage. Moreover, the active sites might react not only with the hydrogen ions but also with other ions present in the measured solution, the so-called disturbing ions. All these chemical reactions occurring at the phase boundary are reversible and described by the dissociation constant  $k$ , which is temperature dependent as well.

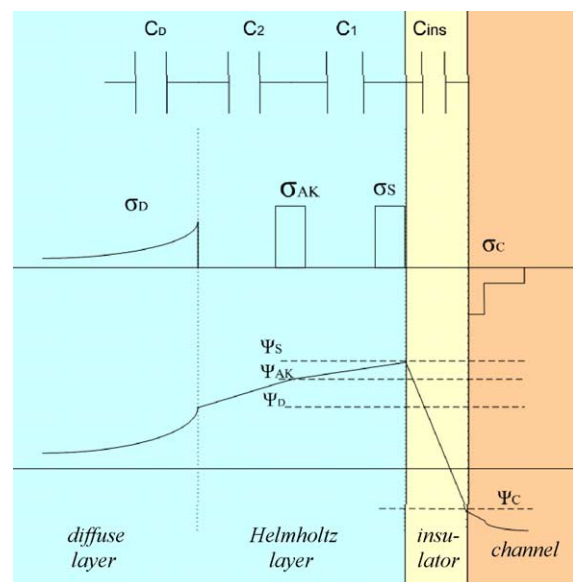


Fig. 2. Charge and potential distribution in the double layer at solid–liquid interface.

Because of the binding of the ions with the active sites, the gradient of ion concentration is created in the electrolyte and, according to the Guy–Chapman–Stern theory, the so-called double layer is established at the dielectric-electrolyte border as it is shown in Fig. 2.

The double-layer consists of the diffuse layer and the Helmholtz layer. The Helmholtz layer comprises the layer of adsorbed hydrogen ions and the common plane of adsorbed anions and cations. The electrical representation of the double layer is also shown in Fig. 2. The letters  $C$ ,  $\sigma$  and  $\psi$  denote the capacitance per unit area, the charge per unit area and the potential, respectively. The indexes D, AK, S, C and ins refer to the diffusion layer, the common plane of disturbing anions or cations, the insulator surface, the transistor channel and the gate insulator, respectively. Based on the theory, assuming that the number of active sites on the surface of the insulator is constant, the system of nonlinear equations, presented further on, describes the relation between all the considered quantities. More details on the theory of charge and potential distribution in the double layer and the derivation of the equations can be found in [4–6].

$$\sigma_D = -\sqrt{8kT\varepsilon_r\varepsilon_0([K_{AK}^+] + [H_S^+])} \times \sinh\left(\frac{ze\Psi_D}{2kT}\right) \quad (1a)$$

$$\sigma_{AK} = e \cdot ([K_{AK}^+] - [A_{AK}^-]) \cdot N_{AV} \cdot S \quad (1b)$$

$$\sigma_S = e \cdot N_{SIL} \cdot \frac{([H_S^+][H_S^+] - k_a k_b)}{([H_S^+]k_b + (1 + k_{aip}[A_{AK}^-])[H_S^+][H_S^+] + k_a k_b + k_{kip}k_a k_b [K_{AK}^+])} + e \cdot N_{NIT} \left(\frac{[H_S^+]}{[H_S^+] + k_n}\right) \quad (1c)$$

$$\sigma_C = \sqrt{2\varepsilon_S\varepsilon_0kT \left[ p_0 \left( \exp\left(\frac{-e\Psi_S}{kT}\right) + \frac{-e\Psi_S}{kT} + 1 \right) + n_0 \left( \exp\left(\frac{e\Psi_S}{kT}\right) - \frac{e\Psi_S}{kT} - 1 \right) \right]} \quad (1d)$$

$$\sigma_S + \sigma_C + \sigma_{AK} + \sigma_D = 0 \quad (1e)$$

$$\Psi_S - \Psi_{AK} = -\frac{\sigma_{AK}}{C_1} \quad (1f)$$

$$\Psi_{AK} - \Psi_D = -\frac{\sigma_D}{C_2} \quad (1g)$$

$$\Psi_C - \Psi_S = \frac{\sigma_C}{C_{ins}} \quad (1h)$$

where

- $C_1, C_2, C_{ins}$  layer capacitances [F/m<sup>2</sup>]
- $[H_S^+]$  hydrogen ion concentration at dielectric surface [mole/l]
- $[K_{AK}^+], [A_{AK}^-]$  cation and anion concentration at the common plane [mole/l]
- $N_{AV}$  Avogadro number =  $6.023 \times 10^{23}$  [mol<sup>-1</sup>]
- $N_{SIL}, N_{NIT}$  silane and nitrite active sites density [m<sup>-3</sup>]

$S$	surface area [m <sup>2</sup> ]
$T$	absolute temperature [K]
$c$	total concentration of cations [mol/l]
$e$	electron charge $1.602 \times 10^{-19}$ [C]
$k$	Boltzmann constant $1.38 \times 10^{-23}$ [J/K]
$k_a, k_b, k_n$	silane and nitrite partition constants [–]
$k_{aip}, k_{kip}$	disturbing ions partition constants [–]
$n_0, p_0$	equilibrium electron and hole concentration [m <sup>-3</sup> ]
$z$	ion electrovalence [–]
$\varepsilon_0$	vacuum electric permittivity $8.85 \times 10^{-12}$ [F/m]
$\varepsilon_r$	electrolyte relative electric permittivity [–]
$\varepsilon_s$	silicon relative electric permittivity [–]

The solution of the above set of equations leads to the computation of the dependence of the insulator surface potential  $\psi_s$  on the hydrogen ion concentration pH. The obtained theoretical solution for different values of the disturbing ion concentration pA or pK is presented in Fig. 3. As can be observed in the chart, the disturbing ions cause the characteristics to flatten out both for high and low values of the hydrogen ion concentration. Then, the device becomes practically insensitive to the hydrogen ion concentration. Fortunately, this is true only for very high concentration values of the disturbing ions. For example, when the

concentration of the disturbing ions pA or pK at the common plane (see Fig. 2) is equal to 1 (thick black line), the measurement range is limited to pH between 2 and 10. On

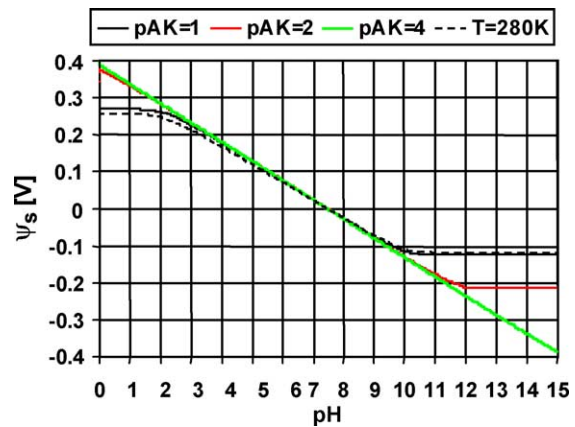


Fig. 3. Theoretical dependence of insulator surface potential on hydrogen and disturbing ion concentration.

the other hand, when  $pAK$  equals 4 (light gray line), the influence of the disturbing ions is negligible.

Additionally, the influence of temperature was also visualised in the figure. Namely, the thinner black line was obtained for a temperature value of 280 K, whereas the remaining curves were computed at a temperature of 300 K. As can be seen, the temperature changes the slope of the curve and consequently the device sensitivity, rather than the location of the bending points. Moreover, it should be underlined that the presented results were obtained for some model parameter values reported in the literature. Nevertheless, all the presented considerations should remain valid for real devices. The computed from the model values of the surface potential  $\psi_s$  will be used to modify the transistor threshold voltage in the subsequent electrical simulations according to the following formula:

$$V_T^{ISFET} = V_T^{MOS} - \psi_s + \text{const} \quad (2)$$

where

$V_T^{ISFET}$ ,  $V_T^{MOS}$  ISFET and MOSFET threshold voltages [V]  
const is constant representing all the potential drops independent from the ion concentration.

#### 4. Semiconductor model

Most of the physical phenomena occurring in the semiconductor part of the ISFET sensor are already modelled in the well-known SPICE environment. Thus, the authors decided to adapt the existing SPICE MOSFET model for the overall chemo–thermo–electrical simulations of the device. As it was already mentioned, the only quantity relating the earlier described model of the phenomena occurring over the device gate is the surface potential  $\psi_s$ , which modifies the transistor threshold voltage. This approach is not entirely new and was proposed already in the early 1990s, e.g. in [7]. Thus, the proposed by the authors ISFET model can be regarded as an extended SPICE MOS transistor model. Because, as it is demonstrated in the later presented measurements, temperature plays an important role in the device operation, the particular stress has been laid on the proper modelling of the temperature phenomena in the device.

Fig. 4 summarises the most important factors influencing the ISFET operation from the thermal point of view. Some of the thermal dependencies, such as the change of the thermal potential, were already taken into account in Eqs. (1) and visualised in Fig. 3. Thus, it remains only to analyse how temperature influences the electrolyte, the reference electrode potential and the MOS transistor itself.

First, the dissociation constants for the solutions present in the electrolyte depend strongly on the absolute temperature as follows:

$$k(T) = k(300)^{300/T} \quad (3)$$

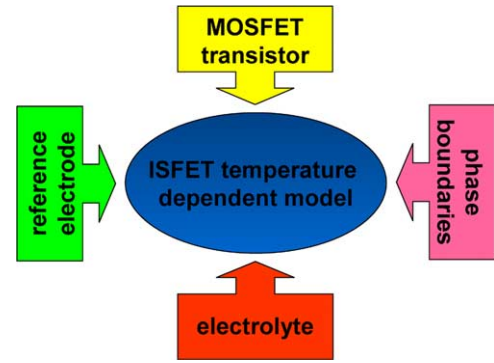


Fig. 4. Factors influencing ISFET thermal behaviour.

Next, the potential of the reference electrode  $E_{ref}$  is assumed to be a sum of the electrode material dependent potential  $E_0$  and some absolute temperature dependent component, as it is shown in the following equation

$$E_{ref} = E_0 + E_T(T - 300) \quad (4)$$

Where the semiconductor part of the device is concerned, the initial simulations demonstrated that the simple Level 1 SPICE MOSFET model was not accurate enough. Therefore, for the actual device simulations a simplified version of the third level SPICE model was employed. The fact that the transistor under consideration had a relatively wide and long channel allowed a simplification of the model by neglecting most of the short channel effect related terms. Then, the transistor drain current can be described by the following equation

$$I_D = \frac{C_{ox}\mu_{eff}}{2} \frac{W_{eff}}{L_{eff}} (2(V_{GS} - V_T) - V_{DS})V_{DS} \quad (5)$$

where

$I_D$  transistor drain current [A]  
 $C_{ox}$  gate dielectric capacitance per unit area [F/m<sup>2</sup>]  
 $\mu_{eff}$  effective carrier mobility [m<sup>2</sup>/Vs]  
 $W_{eff}$  effective channel width [m]  
 $L_{eff}$  effective channel length [m]  
 $V_{GS}$ ,  $V_{DS}$  gate-source and drain-source voltages [V]  
 $V_T$  transistor threshold voltage [V]

The major difference between the Level 1 SPICE model and the one employed by the authors is the introduction of variable carrier mobility. The carrier mobility depends on the electric fields generated both by the gate and the drain potentials. Then, the effective carrier mobility  $\mu_{eff}$  can be expressed by the following equation

$$\mu_{eff} = \frac{\mu_s}{1 + \mu_s \frac{V_{DS}}{v_{max}L}} \left( \frac{T}{T_0} \right)^{-a} \quad (6)$$

where:

$$\mu_s = \frac{\mu_0}{1 + \theta(U_{GS} - V_T)} \quad (7)$$

The quantity  $v_{\max}$  is the maximal carrier velocity.  $T_0$  is the reference absolute temperature.  $\mu_0$  is the low electric field carrier mobility.  $a$  is the mobility thermal dependence coefficient and  $\theta$  is the empirical mobility modulation coefficient, whose dependence on temperature is described by the following relation:

$$\theta(T) = \theta_0 \left( 1 + 1.915 \left( \frac{T}{T_0} - 1 \right) \right) \quad (8)$$

When the transistor is operating in the saturation region, the actual drain-source voltage  $V_{DS}$  is substituted by the saturation voltage  $V_{DSsat}$  expressed by:

$$V_{DSsat} = V_{GS} - V_T + v_{\max} \frac{L_{\text{eff}}}{\mu_{\text{eff}}} - \sqrt{(V_{GS} - V_T)^2 + \left( v_{\max} \frac{L_{\text{eff}}}{\mu_{\text{eff}}} \right)^2} \quad (9)$$

Additionally, it was assumed that in the saturation region the transistor channel effective length  $L_{\text{eff}}$  decreases with the drain-source voltage according to the following formula

$$L_{\text{sat}} = L_{\text{eff}} - \alpha \sqrt{V_{DS} - V_{DSsat}} \quad (10)$$

where  $\alpha$  is the channel length modulation coefficient [ $\text{m}/\text{V}^{0.5}$ ].

The modelling of the dependence of the device threshold voltage  $V_T$  on temperature is a more complex task. This is due to the fact that this voltage, expressed by Eq. (11), is a function of various temperature dependent quantities such as the Fermi level, the intrinsic carrier concentration and the energy band gap.

$$V_T^{\text{MOS}} = V_{\text{FB}} + \gamma \sqrt{2|\Phi_F|} + 2|\Phi_F| \quad (11)$$

where

- $V_{\text{FB}}$  flat-band voltage [V]
- $\gamma$  body effect coefficient [ $\text{V}^{1/2}$ ]
- $\Phi_F$  Fermi potential [V]

The temperature  $T$  affects the flat-band voltage  $V_{\text{FB}}$  through the change of the Fermi potential  $\Delta\Phi_F$  and the band gap  $\Delta W_g$  according to the formula:

$$V_{\text{FB}}(T) = V_{\text{FB}}(T_0) + \frac{1}{2}(\Delta 2|\Phi_F| - \Delta W_g) \quad (12)$$

The value of the energy band gap  $W_g$  expressed in eV can be computed in silicon for different temperature values as:

$$W_g(T) = 1.16 - \frac{7.02 \times 10^{-4} T^2}{1108 + T} \quad (13)$$

Whereas the value of the Fermi level is equal to:

$$\Phi_F(T) = (kT/q) \ln \left( \frac{N_{\text{SUB}}}{n_i} \right) \quad (14)$$

Thus, the Fermi potential is a function of the substrate dopant concentration  $N_{\text{SUB}}$  and the intrinsic semiconductor

carrier concentration  $n_i$ , which in turn is also strongly temperature dependent:

$$n_i(T) = 9.65 \times 10^{15} \left( \frac{T}{T_0} \right)^{3/2} \exp \left( -\frac{W_g}{2kT} + \frac{W_{g0}}{2kT_0} \right) \quad (15)$$

Finally, for the device simulation purposes, Eq. (2) could be transformed to the form shown in Eq. (16), which allowed the computation of the ISFET threshold voltage  $V_T^{\text{ISFET}}$  using the above-described models. This formula takes into account the change with temperature both of the MOS transistor threshold voltage  $\Delta V_T^{\text{MOS}}$  and of the dielectric surface potential  $\Psi_s$ . The value of the MOS transistor threshold voltage  $\Delta V_T^{\text{MOS}}$  at the reference temperature  $T_0$  is estimated based on the measurements.

$$V_T^{\text{ISFET}} = V_T^{\text{MOS}}(T_0) + \Delta V_T^{\text{MOS}}(T) - \Psi_s(T, \text{pH}) + \text{const} \quad (16)$$

The change of the MOS transistor threshold voltage with temperature equals to:

$$\Delta V_T^{\text{MOS}}(T) = 3\Delta|\Phi_F| - \frac{1}{2}\Delta W_g + \gamma\Delta\sqrt{2|\Phi_F|} \quad (17)$$

The computed values of the MOS transistor threshold voltage change with temperature for the surface capacitance of the gate dielectric  $C_{\text{ox}}$  equal to  $460 \mu\text{F}/\text{cm}^2$ , which is close to the actual one, are shown in Fig. 5. The reference temperature was equal to  $25^\circ\text{C}$ .

Analysing the above presented formulae, it should be emphasized that, at least theoretically, the rate of the threshold voltage change with temperature can be adjusted through a variation of the substrate doping and the gate material capacitance (change of material or its thickness). More detailed considerations on the theory of the ISFET electro-thermo-chemical model can be found in [8].

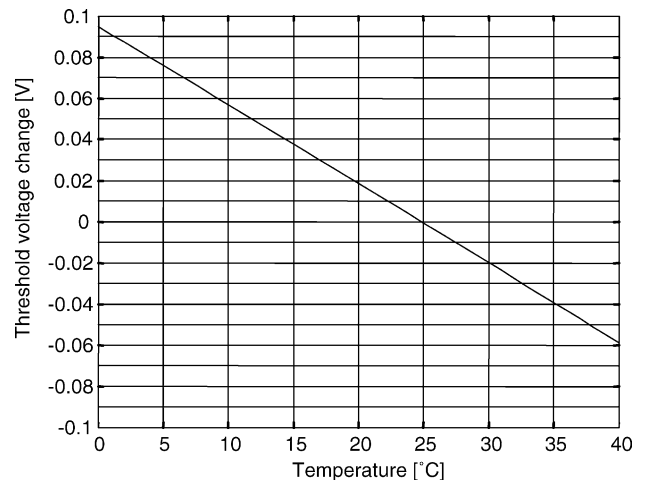


Fig. 5. Theoretical change of threshold voltage with temperature ( $T_0 = 25^\circ\text{C}$ ).

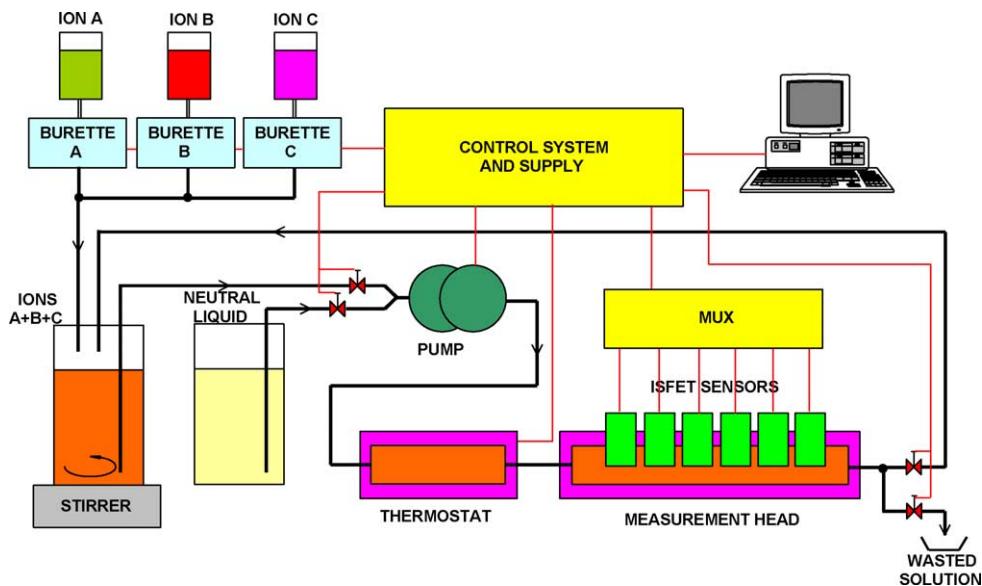


Fig. 6. WUT data acquisition system.

5. Measurements

The device model presented in the previous sections was validated performing electrical measurements and simulations of two different real ISFET structures. The ISFETs of the first type were manufactured at the Institute of Electron Technology (IET) in Warsaw, Poland. The transistors have a built-in n-type channel 640 μm wide and 14 μm long. The other transistors were manufactured at the Laboratoire d'Analyse et d'Architecture des Systèmes (LAAS) in Toulouse, France. These devices are n-type enhancement mode transistors with the channel size 800 × 40 μm. Except for the fact that the IET ISFETs have a built-in channel, the main difference between the devices is that the IET sensors have back side contacts and can be directly submerged in the analysed solution. On the contrary, the LAAS transistors have front side contacts and have to be placed in special packages called dipstick.

The measurements of the IET ISFETs were performed on the especially designed stand described in [9]. The design of this stand, outlined in Fig. 6, allows fully automated measurements of the transistor characteristics for various

ion concentrations and different temperatures. The measurements of the LAAS sensors were performed using a different measurement stand designed at the Department of Microelectronics and Computer Science in Lodz, Poland. This stand, as shown in Fig. 7, consists of a PC equipped with the NI6025E Data Acquisition Board connected directly to the ISFET operating circuit. Additionally, the special software rendering possible automatic sensor measurement has been developed in the LabVIEW environment. Besides, the stand comprised an electromagnetic stirrer and a thermostat. Owing to this design, the measurements can be precisely controlled ensuring stable device polarisation and efficient data acquisition.

The measurements were performed simultaneously for several ISFETs of each kind with variable hydrogen ion concentrations and for different temperatures. For the measurements, in order to guarantee a constant and known hydrogen ion concentration, special buffered solutions were used. Before the measurements all the sensors were conditioned for several hours in deionised water so as to eliminate the so-called base line drift phenomenon. The average measured output characteristics are shown

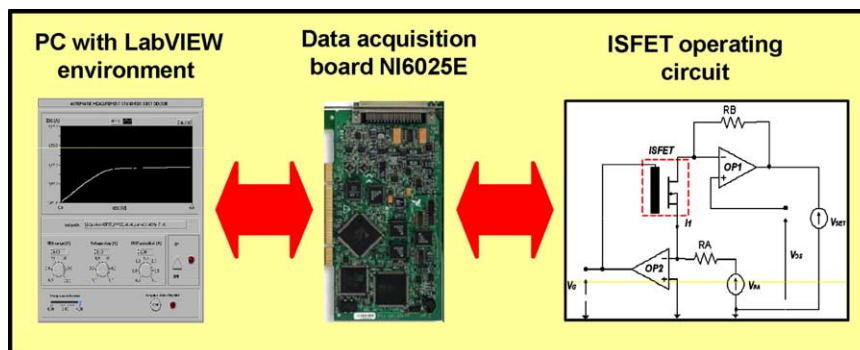


Fig. 7. DMCS data acquisition system.

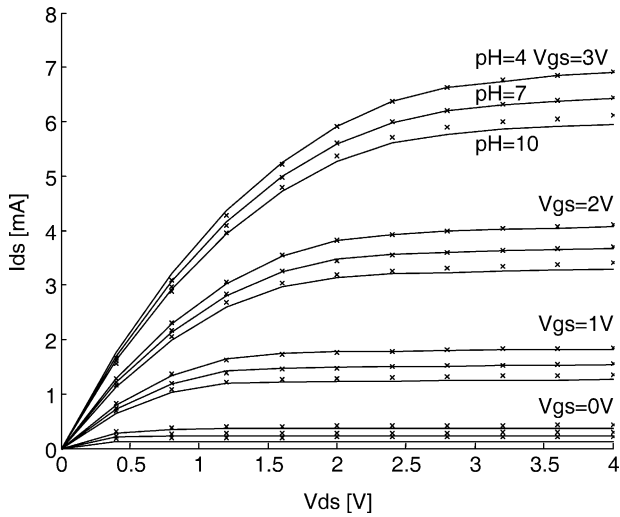


Fig. 8. Output IET ISFET characteristics:  $T=25\text{ }^{\circ}\text{C}$ .

both of the IET and LAAS sensors together with the simulation results in Figs. 8 and 9 and in Figs. 10–12, respectively. The measured values are represented in the figures by crosses.

All the measured ISFET sensor characteristics were in accordance with the earlier presented theoretical considerations. Additionally, the measurements proved the thesis that temperature influences significantly the ISFET operation. The measured device sensitivity to temperature depends strongly on the transistor operating point. Namely, in the case of the IET ISFET, for the  $V_{GS}$  voltage equal to 3 V the variation of the saturation drain current  $I_{DSsat}$  is 141  $\mu\text{A}$  per decade of pH and 27  $\mu\text{A}$  per degree Celsius. When  $V_{GS}$  equals 1 V these values drop down to 84  $\mu\text{A}$  and 7  $\mu\text{A}/\text{K}$ , respectively. This means that at high gate bias the change of the hydrogen ion concentration by a decade (10 times) produces similar response as the change of temperature by 5 K whereas at moderate gate bias the equivalent change of temperature increases to almost 13 K.

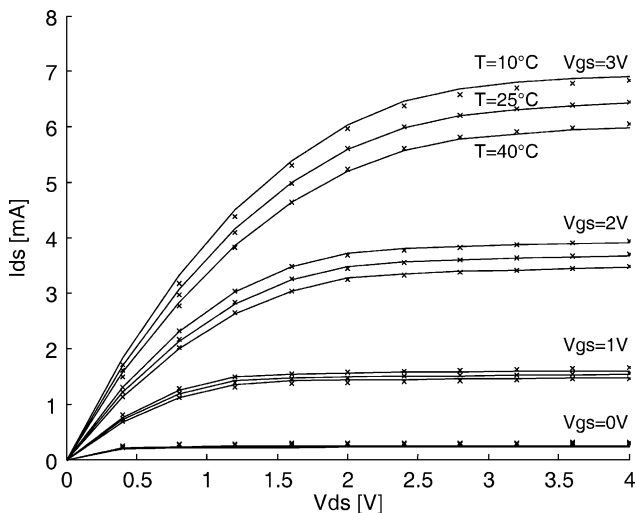


Fig. 9. Output IET ISFET characteristics:  $\text{pH}=7$ .

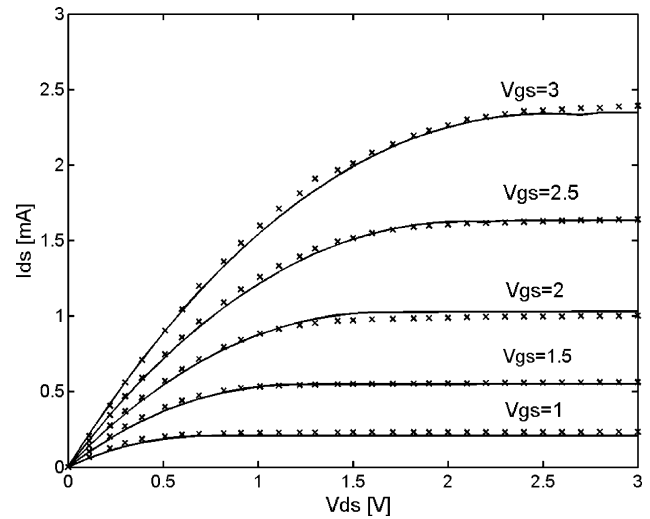


Fig. 10. Output LAAS ISFET characteristics:  $\text{pH}=7$ ,  $T=25\text{ }^{\circ}\text{C}$ .

The LAAS ISFETs also exhibited a quite high sensitivity to temperature. In this particular case, the change of temperature producing the same effect as the change of ion concentration by a decade of pH equalled 6 K at  $V_{GS}$  equal to 2 V and increased to 12 K for  $V_{GS}$  equal to 1 V. Thus, one can state that the optimal bias of the gate electrode is around 1 V over the threshold voltage. Then, the sensitivity to the hydrogen ions is high while the temperature sensitivity remains quite low. Additionally, the  $V_{DS}$  voltage should not be too high so that to avoid excessive power consumption and device self-heating.

During the measurements, the actual LAAS ISFET sensor sensitivity to the hydrogen ion concentration was also determined. This was done by maintaining the constant sensor current of 100  $\mu\text{A}$  while submerging the devices in different solutions and recording the reference electrode potential change. The investigated hydrogen ion concentrations pH ranged from 1 to 10. Additionally, the measurements were taken also in the presence of some disturbing ions, however these ions had little effect on the measurements. The average sensitivity was estimated based on the measurements as 53 mV/pH, which is very close to the theoretical one.

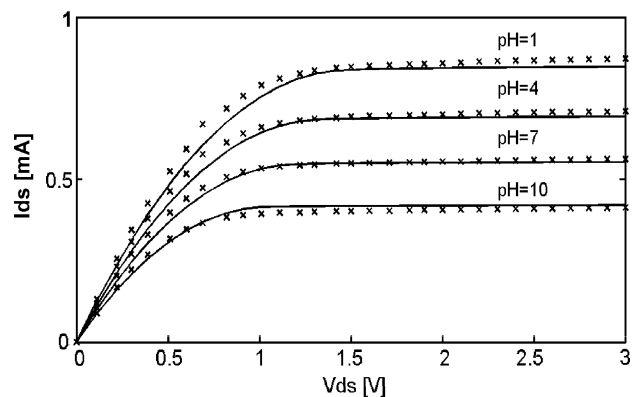


Fig. 11. Output LAAS ISFET characteristics:  $V_{gs}=1.5\text{ V}$ ,  $T=25\text{ }^{\circ}\text{C}$ .

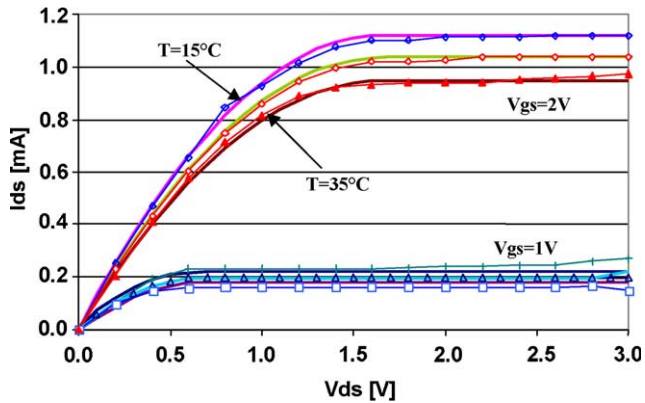


Fig. 12. Output LAAS ISFET characteristics: pH=7.

Unfortunately, due to the construction of the other measurement stand, such a direct sensitivity measurements were not possible with the IET devices. Nevertheless, it was possible to estimate indirectly their sensitivity as slightly more than 53 mV/pH for high hydrogen ion concentrations. However, for pH values around 9–10 the device sensitivity visibly decreases down to only 41 mV per decade. Then, bearing in mind that the pH values are the logarithmic function of hydrogen ion concentration, for low ion concentrations, the ISFET becomes more vulnerable to the presence of other ions than the hydrogen ones. These disturbing ions, as explained in the theoretical part of the paper, bind with the active sites in the gate dielectric instead of the hydrogen ions hence degrading the ISFET sensitivity. This results in the appearance of a bending in the surface potential vs. pH characteristics as it was illustrated in Fig. 3.

Concluding, the sensitivity of investigated devices to the hydrogen ion concentration proved to be satisfactory. Their main drawback is the relatively high sensitivity to temperature. Comparing the two types of sensors, the LAAS ISFETs exhibited better selectivity and repeatability of their characteristics. On the other hand, the IET devices do not require gate polarisation and special packaging. More detailed description of the measurements can be found in [10–11].

## 6. Device simulation

The earlier presented measurements provided the data necessary for the model parameter extraction. The parameters were extracted using a Newton–Gauss method based procedure using the Least Mean Squares criterion so as to find the best possible set of model parameters. The unknown parameters to be determined were the threshold voltage  $V_T$ , the low electric field carrier mobility  $\mu_0$ , the electric field mobility modulation coefficient  $\theta$ , the thermal mobility degradation coefficient  $a$ , the maximal carrier velocity  $v_{max}$  and the gate capacitance per unit area  $C_{ox}$ . The final values of the model parameters adopted for the simulations of both structures are given in Table 1.

Table 1  
Fitted model parameter values

Parameter	IET	LAAS	Unit
Threshold voltage $V_T$	-0.54	0.22	[V]
Low electric field mobility $\mu_0$	680	890	[cm <sup>2</sup> /Vs]
Electric field mobility modulation coefficient $\theta$	0.017	0.022	[1/V]
Thermal mobility degradation coefficient $a$	1.7	1.5	[-]
Maximal carrier velocity $v_{max}$	$4.5 \times 10^4$	$3.0 \times 10^4$	[m/s]
Gate capacitance per unit area $C_{ox}$	440	435	[ $\mu\text{F}/\text{cm}^2$ ]

The simulation results obtained using these parameters are visualised with solid lines in Figs. 8–12.

As can be seen from the figures, the fitted curves match quite accurately the measured values. The value of the average mean squared error related to the measured values does not exceed 5%. Taking into account that the proposed model is relatively simple, the simulation results are satisfactory. Moreover, the model parameter values presented in the table are close to the default ones built in the SPICE simulator. The values of the transistor threshold voltages and the gate dielectric capacitances for both devices are almost identical to the values computed based on the technological data.

## 7. System simulation

The presented ISFET model, as already mentioned, can be implemented without any difficulties in some Hardware Description Language (VHDL-AMS or Verilog-A) which allows multidomain behavioural simulations of complex microsystems. The multidomain behavioural simulators have many advantages. First of all, both the analogue and the digital components of a system can be simulated in a single environment. Moreover, if required, some thermal, mechanical or chemical sensors might be incorporated in the simulations as well. In this particular paper, the previously described ISFET model was implemented using the VHDL-AMS language in the hAMster environment for multidomain simulations of a system consisting of the sensor itself and a data processing unit containing a sigma-delta analogue-to-digital converter ( $\Sigma$ - $\Delta$  ADC) shown in Fig. 13. The system simulated in this section could in turn constitute a part of some larger microsystem.

The  $\Sigma$ - $\Delta$  converter belongs to the group of oversampling converters, which sacrifice the resolution in amplitude for the resolution in time. Owing to this solution, the user can adjust the resolution of the converter to the required accuracy. The converter consists of the analogue  $\Sigma$ - $\Delta$  modulator and the digital decimation filter, hence it has to

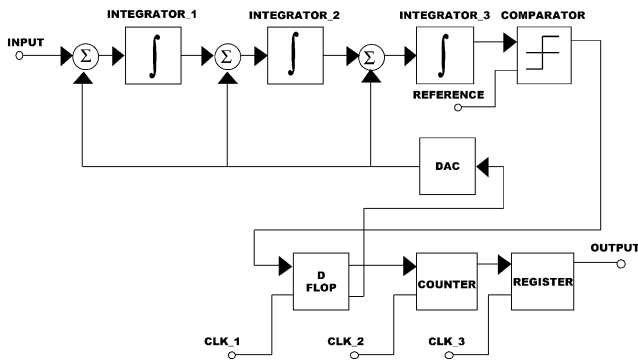


Fig. 13. Block diagram of the data processing unit.

be simulated using design tools capable of mixed-signal simulations.

There exist many possible architectures for the  $\Sigma$ - $\Delta$  modulators, which were explored extensively in literature [12–16]. The authors themselves also studied numerous converter realisations of the 1st–4th order. Generally, the increase of the modulator order improves the signal-to-noise ratio but it might cause some problems with stability as well. Finally, the 3rd order  $\Sigma$ - $\Delta$  converter, whose block diagram is also shown in Fig. 13, was adopted for the simulations. As can be seen the converter has three integrator blocks in the main signal path of the modulator, hence its name. The entire modulator model consists of separate blocks, including the integrators, the comparator, the D flip-flop, the digital-to-analogue converter and the summation nodes connected together using structural description in VHDL-AMS language.

The second part of the presented ADC is the digital decimation filter. The filter converts a one-bit binary stream representing the amplitude of the input signal into n-bit binary words. The considered implementation of this unit uses a 12-bit counter as an averaging filter, which returns the average value of the  $\Sigma$ - $\Delta$  modulator output over a fixed period.

The counter operating at the oversampling frequency produces an 12-bit binary word. This word is loaded into the output register, which is the output signal of the whole ADC. The main disadvantage of this solution is that

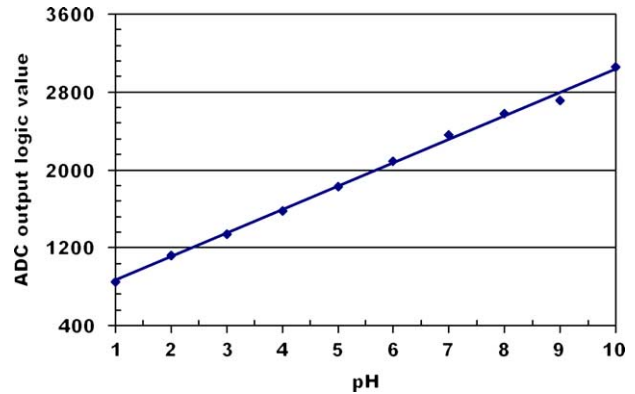


Fig. 15. Results of the system simulations.

the increase of the ADC resolution requires the increase the oversampling frequency.

Thus, the ADC is much easier to model with VHDL-AMS because it consists only of two building blocks, the 12-bit counter and the 12-bit register, which form the decimation filter and can be connected to the earlier described  $\Sigma$ - $\Delta$  modulator. The behaviour of the 3rd order  $\Sigma$ - $\Delta$  ADC was tested using the sinusoidal input signal. The obtained simulation results are shown in Fig. 14.

Finally, the entire microsystem was fully simulated using the VHDL-AMS models of the presented structures. The input system signal for these multidomain simulations is the hydrogen ion concentration and the output system signal is the digital value stored in the output ADC register. The results of the simulations are presented in Fig. 15. The resolution of the converter can be estimated dividing the maximum range of input signal, e.g. 1 V by the maximal number of logic levels (4096 for 12 bit), which gives approximately 0.24 mV. This value corresponds to the resolution of about 0.005 pH in terms of the hydrogen ion concentration. The slight nonlinearities present in the output system signal are mainly due to the nonlinearity introduced by the signal processing unit. It should be underlined that the converter resolution can be adjusted by varying the length of the converter. More detailed presentation of the simulations together with the analysis of different realisations can be found in [17].

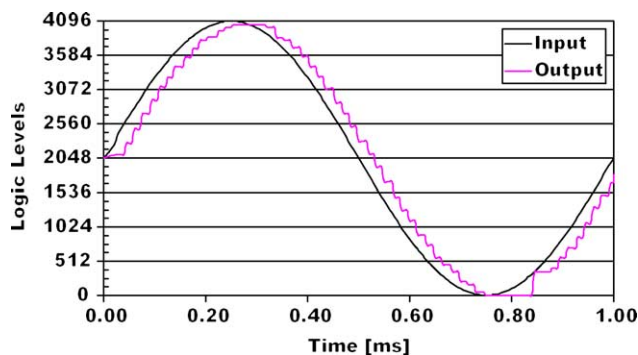


Fig. 14. Simulation results of the  $\Sigma$ - $\Delta$  ADC.

## 8. Conclusions

This paper presented a relatively simple, but accurate temperature dependent model of the ISFET sensor. The proposed model is based on a modified SPICE MOS transistor model in which the threshold voltage is influenced by the gate surface potential induced by hydrogen ions present in the electrolyte flowing over the gate structure. The model combines in a single set of mathematical equations different chemical, thermal and electrical phenomena occurring in the device. In spite of its apparent complexity, the number of model parameters necessary for

simulations is fairly low. The proposed model is suitable for the simulations of the device operating in a relatively wide range of temperatures and hydrogen ion concentrations. Moreover, when the electro-chemical model of the phenomena occurring in a particular ion selective membrane is known, the presented model can be easily adapted and applied for the analysis of any other FET-based ion sensor (CHEMFET) as well.

The proposed model was successfully employed for the simulation of real devices. The model parameters were determined based on the measurements. The simulations performed for the extracted parameter values showed good agreement with the measurements. Additionally, both the measurements and the simulations demonstrated clearly that temperature has significant influence on the device performance. The sensitivity to temperature can be controlled to some extent by the proper choice of the substrate doping, the gate dielectric material and the device operating point.

Moreover, the model was straightforwardly implemented in the VHDL-AMS language. Owing to this solution it was possible to perform in a single environment multidomain mixed mode simulations of the more complex system containing the ISFET sensor and the data processing unit.

The main advantage of the VHDL-AMS simulations at the system level is the possibility of reducing significantly the design cost and the simulation time comparing to the traditional transistor level simulations. In the case presented here, the whole microsystem was fully designed and tested using the VHDL-AMS language. Moreover, different  $\Sigma$ - $\Delta$  AD converter structures were compiled in silicon in the CADENCE environment as a real reconfigurable integrated circuit and shipped for manufacturing in 0.6  $\mu\text{m}$  AMS technology.

## Acknowledgements

The presented research was supported by the 5th European Framework Programme project SEWING-System for European Water monitoring IST-2000-28084 and the grants of the Polish State Committee for Scientific Research No. 4 T11B 012 24 and No. 4 T11B 014 24.

The authors would like to extend their gratitude to all the SEWING partners, especially to the project co-ordinator Prof. Filipkowski from the Institute of Electronics Systems at the Warsaw University of Technology, and Prof. Jachowicz, Dr Weremczuk and Mr. Sochon from the same Institute for their help in the measurements. Special thanks are also directed towards Prof. Brzozka, Prof. Wroblewski and Prof. Dybko from the Institute of Chemistry at the Warsaw University of Technology for the fruitful discussions concerning modelling of the chemical phenomena and preparation of the electrolytes.

## References

- [1] L.K. Meixner, S. Koch, Simulation of ISFET operation based on the site binding theory, *Sens. Actuators B* 6 (1992) 315–318.
- [2] C.D. Fung, P.W. Cheung, A generalized theory of an electrolyte-insulator-semiconductor field effect transistor, *IEEE Trans. Electron Devices* 33 (1) (January 1986) 8–18.
- [3] J. Ogrodzki, L. Opalski, Modeling of semi-conductor pH sensors for CAD, Proceedings of the 7th International Conference Mixed Design of Integrated Circuits and Systems-MIXDES 2000, 15–17 June, 2000, 259–264.
- [4] R.H. Kingston, S.F. Neustadter, Calculation of space charge, electric field and free carrier concentration at the surface of a semiconductor, *J. Appl. Phys.* 26 (1955) 718–720.
- [5] D.E. Yates, S. Levine, T.W. Healy, Site-binding model of the electrical double layer at the oxide water interface, *J. Chem. Soc. Faraday Trans. I* 70 (1974) 1807–1818.
- [6] M. Daniel, M. Szermer, A. Napieralski, W. Wróblewski, A. Dybko, Ion-selective sensors modeling for CAD, 9th International Conference Mixed Design of Integrated Circuits and Systems-MIXDES 2002, 20–22 June 2002, Wrocław, Poland, pp. 147–150.
- [7] M. Grattarola, G. Massobrio, S. Martinoia, Modelling H<sup>+</sup> sensitive FET's with SPICE, *IEEE Trans. Electron Devices* 39 (4) (1992) 813–819.
- [8] M. Janicki, M. Daniel, A. Napieralski, Modelling of temperature phenomena in ion sensitive transistors, Proceedings of the 9th International Workshop on Thermal Investigations of ICs and Systems THERMINIC', Aix-en-Provence, France, 24–26 September 2003, pp. 335–340.
- [9] R. Jachowicz, J. Weremczuk, J. Sochoń, Automatic stand for IS-FET sensors parameters identification, Proceeding of the 9th International Conference Mixed Design of Integrated Circuits and Systems-MIXDES 2002, Wrocław, Poland, 20–22 June 2002, pp.199–202.
- [10] M. Janicki, M. Daniel, A. Napieralski, Parameter extraction for electro-chemical simulations of ion sensitive transistors, Proceedings of the 10th International Conference Mixed Design of Integrated Circuits and Systems MIXDES'2003, Lodz, Poland, 26–28 June, 2003, pp. 450–455.
- [11] M. Daniel, M. Janicki, A. Napieralski, Simulation of ion sensitive transistors using a spice compatible model, Proceedings of the 2nd IEEE International Conference on Sensors IEEE Sensors, Toronto, Canada, 22–24 October 2003, pp. 596–597 (abstract).
- [12] A.S. Botha, P. Sniatala, HDL-A description of a/d converter based on delta-sigma modulator, Proceedings of the 9th Mixed Design of Integrated Circuits and Systems Conference MIXDES', Wrocław, Poland, 2002, pp. 447–451.
- [13] R. Baraniecki, P. Dabrowski, K. Hejn, Oversampling  $\sigma\Delta$  analog-to-digital converter modeling based on VHDL, *Analog Integr. Circuits Signal Process* 16-2 (1998) 101–109.
- [14] N. Tan, *Switched-Current Design and Implementation of Oversampling A/D Converters*, Kluwer Academic Publishers, Dordrecht, 1997.
- [15] P.J. Crawley, G.W. Roberts, Switched-current sigma-delta modulation for a/d conversion, Proceedings of the IEEE International Symposium on Circuits and Systems, San Diego, CA, USA, 1992, 1320–1323.
- [16] J.C. Candy, G.C. Temes, *Oversampling Delta-Sigma Data Converters: Theory Design and Simulation*, Wiley/IEEE Press, New York, 1991.
- [17] M. Szermer, M. Daniel, A. Napieralski, Design and Modelling of Smart Sensor Dedicated for Water Pollution Monitoring, Proceedings of the 2003 Nanotechnology Conference NANOTECH 2003, vol. 1, San Francisco, CA, USA, 2003, pp. 110–114.